1003D), which were removed from the animals 24 h after the implantation, followed by withdrawal of PTH treatment for 6 days. In this regimen, the dose of PTH was 1.67 μg/kg/0.9 μl/h, which is equivalent to 40 μg/kg/24 h. Each osmotic pump was filled up more than 6 h before implantation and stored in sterile saline at 37°C so that pumping could be initiated immediately after implantation. The total amount of PTH administrated was identical for all the injection and infusion groups (40 μg/kg/week), except for the C280-PTH group (280 μg/kg/week).

Serum calcium levels were measured for 1 week during the various PTH treatments described above. All of the PTH treatments induced no significant differences in body weight gain as compared with the control rats (data not shown).

Measurement of serum calcium

Under ether anesthesia, approximately 200 μl of blood was obtained from the subclavian vein immediately before and 24, 48, 72, and 168 h after implantation or the first injection of PTH. The blood was centrifuged, and the serum was stored at −80°C. Total serum calcium was determined using an automated analyzer (Super Z818; MC Medical, Tokyo, Japan) and the Calcium E-HA test Wako (Wako Pure Chemical Ind. Ltd., Tokyo, Japan).

Preparation of bone samples

Calcein (10 mg/kg) was subcutaneously administered to all rats on the 10th and 3rd days before death. At the end of the experiment, the animals were anesthetized with diethyl ether and killed by cardiectomy. The right and left femurs and the right tibia were removed. The right and left femurs were stored at −20°C, and the right femurs were analyzed using dual energy X-ray absorptiometry (DXA) and micro-computed tomography (μCT), and left femurs were used for mechanical properties analysis. For bone histomorphometry, the tibiae were fixed for 24 h in 10% phosphate-buffered formalin, which was subsequently replaced with 70% ethanol. Histological sections were obtained as described below.

Measurement of bone mineral density

The bone mineral density (BMD; mg/cm^2) of the right femur was measured using DXA (DCS-600EX-IIIR; Aloka Co. Ltd., Tokyo, Japan) with a scan pitch of 1 mm and a scan speed of 25 mm/s.

μCT analysis

For cortical bone analysis, the midpoint of the femur diaphysis was scanned at a voxel size of 12.5 × 12.5 × 12.5 μm^3 by using μCT (Scan Xmate-RB090SS150; ComscanTechno, Kanagawa, Japan) with an X-ray source of 70 kV/100 μA. The obtained images were reconstructed and processed using 3D image analysis software (TRI/3D-BON; RATOC System Engineering, Tokyo Japan). Four slices (thickness, 50 μm) of bone were examined, and the mean cortical thickness (μm) was measured.

Analyses of the mechanical properties of bones

The cantilever bending strength of the femoral neck was measured according to a previously described method [12] by using a mechanical testing machine (EZ-L-1kN; Shimadzu, Kyoto, Japan); subsequent data were analyzed using this machine's enclosed software package. Before performing the femoral neck compression test, the femora were thawed at room temperature. For the test, the femur was cut at the midpoint of its diaphysis. The proximal part of each specimen was mounted in methacrylate resin (OSTRON-II; GC Dental Products Co., Aichi, Japan) to fix the specimen to the fixation device. The specimen was then placed on the test apparatus, and a vertical load was applied to the top of the femoral head by using a stainless steel cylinder equipped with a small, concave steel cup at its end. The loading was directed parallel to the femoral shaft. On the basis of the load-deformation curve, the maximum load (N), stiffness (N/mm), and energy to fracture (N mm) were recorded.

Bone histomorphometry

The right proximal tibiae were kept in 70% ethanol and prestained with Villanueva bone stain for 72 h. After dehydration, they were embedded in methyl methacrylate (MMA). Frontal sections of the distal tibia (thickness, 5 μm) were obtained using a microtome. Histomorphometric analyses of metaphyseal trabecular bone were performed using the histomorphometric system for trabecular bone (BONE; System Supply, Nagano, Japan). The bone marrow cavity located 620–1240 μm from the growth plate closest to the diaphysis and 310 μm from both sides of the endosteum of the cortical bone was examined (field of view, 310 × 310; magnification, 320).

The following parameters were analyzed according to standard formulae and nomenclature [13]: bone volume/tissue volume (BV/TV [%]), trabecular thickness (Tb.Th [μm]), trabecular number (Tb.N [N/mm]), osteoblast surface/bone surface (Ob.S/BS [%]), number of osteoclasts/bone surface (N.Oc/BS [N/mm]), bone formation rate/bone surface (BFR/BS [mm^3/mm^2/year]), osteoid volume/bone volume (OV/BV [%]), and mineralization lag time (Mlt [days]).

Statistical analysis

All data in the tables and figures are expressed as the mean ± standard error of the mean (SEM). Statistical analysis was carried out using Static Analysis System (SAS) software. The significance of difference was determined using the Dunnett multiple test (in the intermittent treatment group or the continuous treatment group for comparison between C-CON and C40-PTH or C280-PTH) and the Student's *t* test (in the continuous treatment group for comparison between C-CON and C40-PTH or in the continuous-withdrawal treatment group). A p value of <0.05 was considered significant.

Results

Effects of various PTH treatment regimens on serum calcium

Because a critical adverse effect of PTH treatment is the induction of hypercalcemia, we first determined the appropriate PTH-treatment regimens that do not induce hypercalcemic action. As shown in Fig. 1, intermittent PTH injections both once a week (I×1-PTH) and 3 times a week (I×3-PTH) did not induce any increase in serum calcium levels, as compared with those of control rats (I-CON). In contrast, continuous PTH treatment with a high dose of PTH (280 μg/kg/week; C280-PTH) significantly increased the serum calcium levels from day 1 to day 7 during the treatment, resulting in hypercalcemia (defined as a serum calcium level greater than 10.5 mg/dl). Continuous PTH treatment with a dose of 40 μg/kg/week (C40-PTH) transiently increased the serum calcium level only on day 2, as compared with that in control rats, though it was within the normocalcemic range (8.4–10.4 mg/dl). Similarly, continuous PTH treatment for 24 h followed by withdrawal of PTH treatment for 6 days (PTH-WD) increased the serum calcium level only on day 1, but this level was also within the normocalcemic range. Thus, among the PTH treatment regimens described above, a high-dose continuous PTH treatment (C280-PTH) induced apparent hypercalcemia during PTH treatment. We therefore excluded this group from further investigations of bone status.

Effects of various PTH treatment regimens on BMD

Table 2 summarizes the BMD of the entire femur and the proximal, diaphyseal, and distal parts of the femur. Intermittent PTH treatment for 4 weeks with 1 injection per week (I×1-PTH) produced no significant differences in the BMD at each part of the bones measured, but the intermittent PTH treatment for the same period with 3 injections

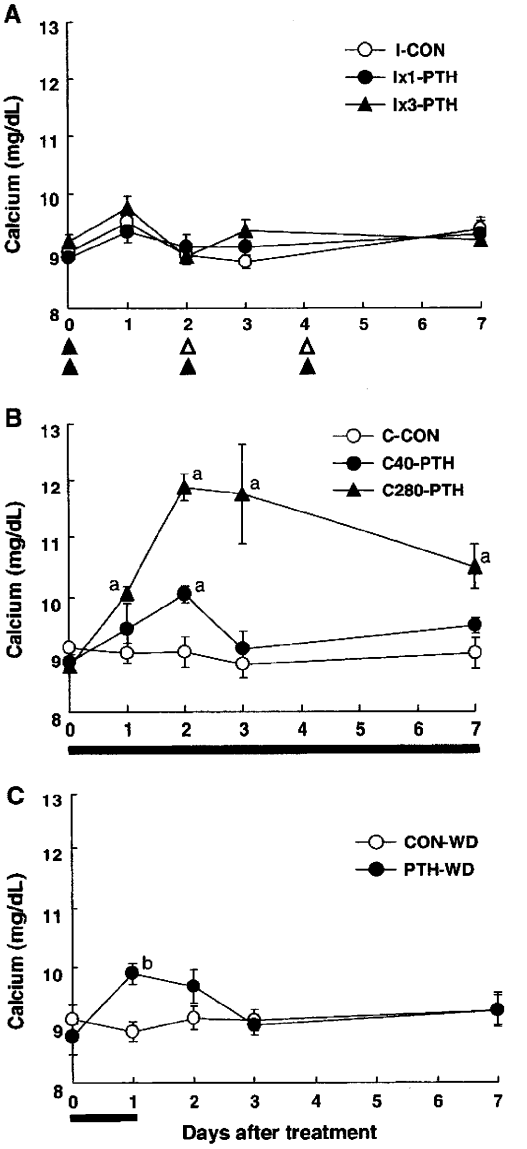

Fig. 1 Serum total calcium in rats treated with intermittent PTH (**a**), continuous PTH (**b**), and continuous PTH withdrawal (**c**). **a** *Solid triangles* indicate the days of PTH injections, and *open triangles* indicate the days of vehicle injections. **b**, **c** The treatment periods are indicated as *black bars*. Values are represented as mean ± SEM ($n = 5$). $^{a}p < 0.05$ vs. C-CON, $^{b}p < 0.05$ vs. CON-WD

per week (I×3-PTH) significantly increased the BMD of the entire femur and the diaphyseal and distal parts of the femur, as compared with that in the corresponding control rats (I-CON). Continuous treatment with PTH (C40-PTH) for 4 weeks significantly decreased the BMD of the entire femur and the proximal region of the femur, as compared with that in the corresponding control rats (C-CON). In contrast, repetitive treatments for 4 weeks with continuous PTH infusion for 24 h followed by withdrawal for 6 days (PTH-WD) significantly increased the BMD in the

Table 2 Bone mineral density of femurs in rats treated with various PTH treatment protocols

	Whole (mg/cm^2)	Proximal (mg/cm^2)	Diaphysis (mg/cm^2)	Distal (mg/cm^2)
I-CON	114.4 ± 1.4	113.8 ± 1.8	105.4 ± 1.5	123.0 ± 1.2
I×1-PTH	118.6 ± 1.7	116.1 ± 1.8	109.8 ± 2.3	128.7 ± 2.2
I×3-PTH	121.7 ± 2.6[a]	119.2 ± 2.7	112.3 ± 1.8[a]	131.9 ± 3.4[a]
C-CON	117.5 ± 1.2	117.2 ± 1.1	109.7 ± 1.9	128.4 ± 3.8
C40-PTH	112.1 ± 1.4[b]	110.8 ± 1.5[b]	104.5 ± 2.1	119.9 ± 1.9
CON-WD	114.4 ± 2.0	111.9 ± 1.5	106.4 ± 1.3	123.4 ± 3.4
PTH-WD	118.4 ± 1.5	118.7 ± 1.7[c]	109.2 ± 1.7	126.2 ± 1.5

Values are expressed as mean ± SEM ($n = 6$). Comparisons of data were performed using Dunnett's test (I-CON, I×1-PTH, and I×3-PTH) and the unpaired t test (C-CON and C40-PTH; CON-WD and PTH-WD)

Significance is indicated by: [a]$p < 0.05$, I×3-PTH vs. I-CON; [b]$p < 0.05$, C40-PTH vs. C-CON; and [c]$p < 0.05$ PTH-WD vs. CON-WD group

proximal region by 6.0%, as compared with that in the control group (CON-WD).

μCT analysis of cortical bone

Both intermittent PTH treatments, i.e., I×1-PTH and I×3-PTH, slightly increased the cortical thickness, but this increase was not significantly different from that observed in the control group (I-CON; Fig. 2). C40-PTH induced no apparent changes in cortical thickness, as compared with those in the control rats (C-CON; Fig. 2). PTH-WD significantly increased the cortical thickness, as compared with that in the control group (CON-WD; Fig. 2).

Bone histomorphometric analyses for cancellous bone

Figure 3 summarizes the results of bone histomorphometric analyses at the metaphyseal region of the proximal tibiae. I×1-PTH induced no significant differences in any parameter, as compared with those in the control rats (I-CON). However, I×3-PTH increased the values of BV/TV, Tb.Th, Ob.S/BS, and BFR/BS, as compared with those in the control rats (I-CON). C40-PTH increased the osteoclast number (N.Oc/BS), but produced no significant differences in the other parameters. PTH-WD significantly increased the OV/BV, Tb.Th, Ob.S/BS, and BFR/BS, as compared with those in the control rats (CON-WD). In the PTH-WD group, a slight but significant decrease in the trabecular number (Tb.N) was also observed. No apparent increase in the N.Oc/BS was observed in this group. We found no significant differences on mineralization lag time (Mlt: O.Th/MAR × OS/MS) among each group (Fig. 3). These data indicate that PTH-WD treatment produces anabolic effects on trabecular bones by stimulating bone formation, without the continuously elevated osteoclastic bone resorption observed in the C40-PTH treatment.

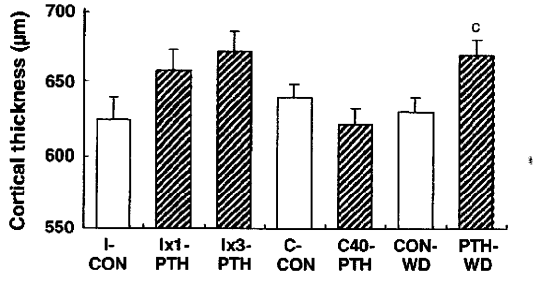

Fig. 2 Cortical thickness of femoral diaphyses measured by micro-CT, as described in "Materials and methods." Values are presented as mean ± SEM ($n = 6$). [c]$p < 0.05$ vs. CON-WD

Mechanical properties of the femoral neck

Table 3 summarizes the mechanical properties of the femoral neck in rats treated with various regimens. I×3-PTH and PTH-WD slightly increased the maximum load, but these values were not significantly different from those in the control rats. The stiffness of the femoral neck tended to be less in the C40-PTH and PTH-WD treatment groups than in each control group. PTH-WD treatment increased the energy required to fracture by 47%, but this value was not significantly different from the values of the control femurs.

Discussion

Various animal experiments have shown that in rats, a continuous infusion of PTH induced catabolic actions in bones, resulting in decreased bone mass and hypercalcemia. However, intermittent treatment with PTH exerted anabolic effects by increasing the bone mass in intact and ovariectomized (OVX) rats and humans [4, 6, 8]. Previous pharmacokinetic studies have indicated that the duration of the serum concentration of PTH above the baseline level of endogenous PTH is a critical factor in regulating such catabolic and anabolic actions on the bone mass [6, 13].

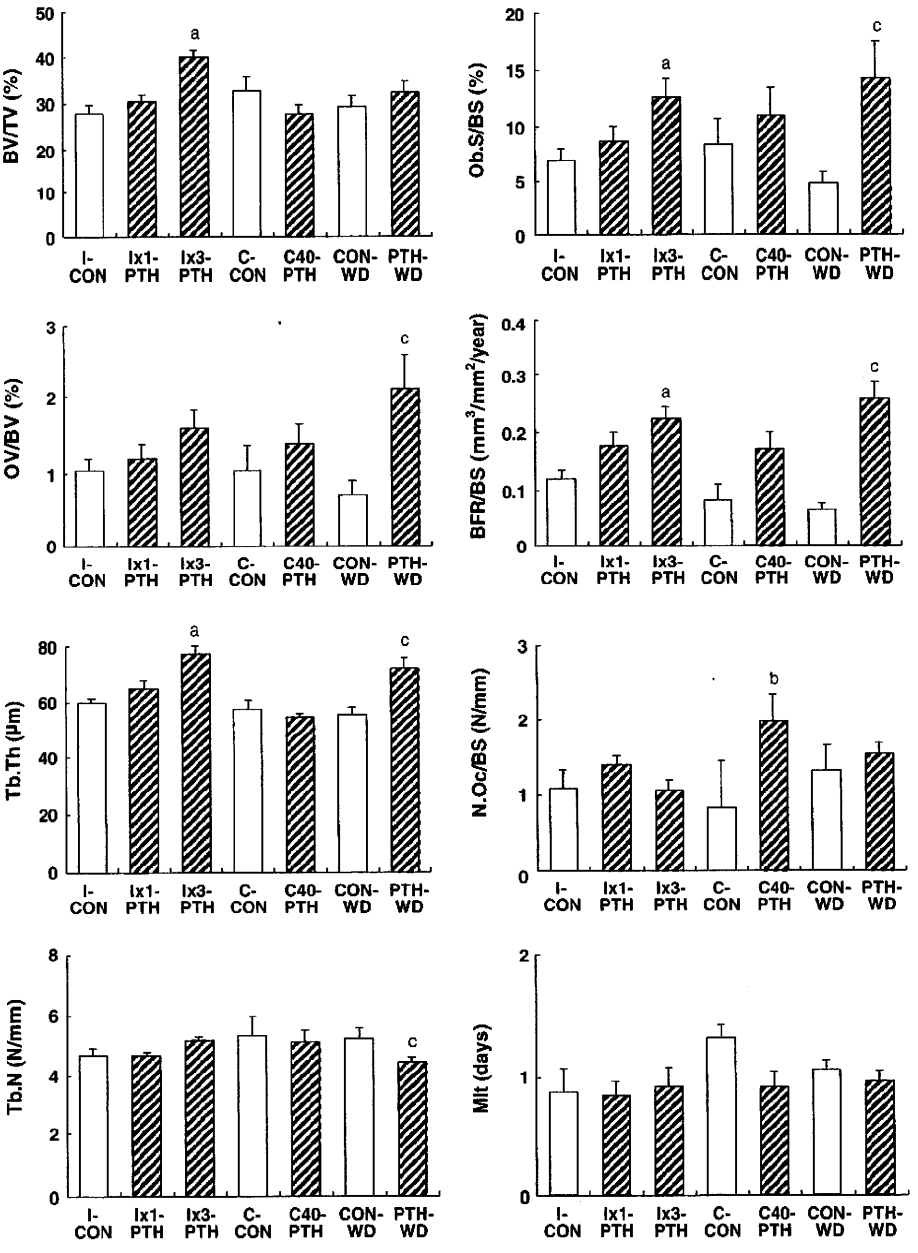

Fig. 3 Histomorphometric indices of trabecular bone in the proximal metaphyses of tibiae in rats treated with various administration regimens for 4 weeks, as described in "Materials and methods". I-CON, intermittent treatment control; I×1-PTH, intermittent injection of PTH once a week; I×3-PTH, intermittent injections of PTH 3 times a week; C-CON, continuous treatment control; C40-PTH, continuous infusion of PTH for 4 weeks; CON-WD, control for PTH continuous treatment followed by PTH withdrawal; PTH-WD, continuous infusion of PTH for 24 h followed by PTH withdrawal for 6 days. Values are presented as mean ± SEM ($n = 6$). $^{a}p < 0.05$ vs. I-CON, $^{b}p < 0.05$ vs. C-CON, $^{c}p < 0.05$ vs. CON-WD

Sustained serum concentration of PTH above the baseline level for more than 6 h per day causes catabolic effects such as decreased bone mass and hypercalcemia; these effects are symptoms of hyperparathyroidism [5, 14]. We showed that the repetition of a continuous infusion of PTH for 24 h followed by a 6-day withdrawal period (PTH-WD) induced some anabolic activity in the bone metabolism, without causing hypercalcemia. This PTH treatment may increase the serum PTH level for more than 6 h on the day of infusion; therefore, a substantial period of withdrawal is important to induce the anabolic effects of PTH in bone metabolism, regardless of continuous treatment with PTH for 24 h. Interestingly, Ishii et al. [15] reported that intermittent lowering of the serum PTH level exerted "anabolic-like" effects on bone mass in rats with chronic renal insufficiency. In their study, intermittent lowering of the serum PTH level increased the trabecular bone thickness, but not the trabecular number; this finding is similar to that observed in the rats of the PTH-WD group in our study. Another study reported that a continuous PTH infusion for 7 days followed by a 21 day withdrawal period increased the mechanical properties of bones [16]; however, the dose

Table 3 Mechanical properties of the femoral head in rats treated with various treatment protocols of PTH for 28 days

	Femoral head compression		
	Maximum load (N)	Stiffness (N/mm)	Energy to fracture (N mm)
I-CON	86.7 ± 5.5	264 ± 27	19.0 ± 2.4
I×1-PTH	82.9 ± 5.0	194 ± 28	23.4 ± 3.6
I×3-PTH	96.8 ± 2.8	304 ± 38	21.0 ± 3.4
C-CON	85.1 ± 5.7	205 ± 13	17.0 ± 3.0
C40-PTH	73.6 ± 3.1	176 ± 23	19.8 ± 2.7
CON-WD	81.2 ± 8.0	273 ± 36	21.4 ± 5.8
PTH-WD	96.1 ± 7.3	172 ± 32	31.3 ± 4.4

Values are expressed as mean ± SEM ($n = 6$). No significance was detected

used in this study (40 μg/kg/day for 7 days) caused transitional hypercalcemia in our experiment (Fig. 1). These results indicate that suitable periods of sustained serum PTH level and PTH withdrawal are important to induce the anabolic effects of PTH on bone, even after continuous PTH treatment.

Our study showed that 4 cycles of PTH-WD treatment as well as I×3-PTH treatment induced some anabolic activity in the bone metabolism. Both treatments increased Tb.Th, Ob.S/BS, and BFR/BS. However, these 2 regimens also produced some other effects. PTH-WD treatment significantly increased the OV/BV, but I×3-PTH treatment failed to significantly increase it. In contrast, PTH-WD treatment failed to increase BV/TV, and I×3-PTH treatment significantly increased it. The Tb.N was maintained in the I×3-PTH group at the level of the control group, but the Tb.N was reduced in the PTH-WD group. This decrease in the Tb.N in the PTH-WD group may be a cause of the non-elevated values of BV/TV, which was observed in the I×3-PTH group. Further, the dissociation between increased Tb.Th and decreased Tb.N in the PTH-WD group will provide important information to understand the action mechanism of PTH-WD treatment. We speculate that the decreased Tb.N might be due to transient or acute bone resorption during continuous PTH treatment for the initial 24 h, though N.Oc/BS was not significantly increased at the end of PTH-WD treatment. Thereafter, active bone formation occurred, and it contributed the increased Tb.Th. Thus, anabolic actions induced by the PTH-WD treatment on the bone structure seem to be different from those observed in the intermittent PTH treatment group without changes in mineralization lag time.

Cortical bone thickness is an important factor that determines the mechanical characteristics of a femur and predicts the bone strength and fracture risk in patients with osteoporosis [17]. Although PTH-WD treatment increased the cortical thickness, the PTH-WD group had mild increases in ultimate force at maximal load without significant differences as well as the I×3-PTH group. The PTH-WD group showed the increase in energy to fracture, but it was not significantly different from other groups. Since PTH-WD treatment failed to induce significant changes in the mechanical properties, it is necessary to conduct long-term studies for more than 4 weeks to record apparent improvements in the mechanical properties.

Continuous PTH treatment as well as intermittent PTH treatment stimulates bone formation, but the former treatment enhances osteoclastic bone resorption that exceeds the stimulated bone formation. In the present study, PTH-WD treatment as well as I×3-PTH treatment prevented increases in the N.Oc/BS, whereas prolonged continuous PTH treatment for 7 days (C40-PTH) significantly increased the N.Oc/BS. These results suggest that a suitable PTH withdrawal period contributes to the induction of anabolic bone action by preventing overstimulation of osteoclastic bone resorption. This assumption is supported by studies that showed that the ratio of the receptor activator of the nuclear factor κB ligand (RANKL) to osteoprotegerin (OPG) (RANKL/OPG ratio) and MCP-1 expression, which are known to be the key regulators of osteoclast differentiation, depend on the exposure time to PTH [18, 19].

The recommended regimen of recombinant human PTH(1-34), Forteo, which is a potent FDA-approved drug for the treatment of osteoporosis, is once a day by self-administered injections. The compliance of patients with this treatment is moderate because of high cost and adverse effects such as pain at the injection site [9, 20, 21]. To overcome these problems, several researchers have attempted the use of less- or noninvasive and inexpensive delivery systems for PTH [11, 22, 23], including an injectable formulation with a low frequency of injection and an oral delivery system. Balck et al. [24] showed that daily injections of PTH (1–84) for a month followed by weekly injections of PTH (1–84) for 11 months increased the vertebral BMD in patients with osteoporosis; this suggests that less frequent PTH injections can be used as an anabolic therapeutic regimen. One of the hurdles in oral administration appears to be the attainment of pulsatile PTH plasma concentrations, which induce anabolic effects in the bone. In the present study, we showed that the repetition of 24-h continuous infusions of PTH followed by 6-day withdrawal periods induced anabolic effects in the bone. Another critical issue that should be considered carefully is the induction of hypercalcemia by PTH administration. Horwitz et al. [25] revealed that continuous infusion of PTH for 23 h did not induce severe hypercalcemia in healthy human volunteers. Our results indicated that continuous PTH infusion for 24 h slightly increased the serum calcium level, which remained lower than the

hypercalcemic level on day 1, and the normocalcemic level was regained from day 2. Since the serum calcium level after the oral administration of PTH will return to normal level within 24 h, oral administration followed by PTH withdrawal will be a potential therapeutic regimen of PTH treatment that can induce anabolic effects in the bone without inducing hypercalcemia.

It is essential to determine the suitable intervals of PTH exposure and withdrawal in order to establish a therapeutic regimen for PTH treatment. Katz et al. [26] reported that in 9- to 13-week-old male rats, the resorption and formation periods are 2.1 days and 14.4 days, respectively, and these periods are prolonged in older rats and humans; therefore, the bone turnover period, expressed as the activation frequency or bone remodeling unit, is a critical factor in determining suitable treatment periods. In addition, this study raised the possibility that variable regimens of PTH treatment regulate osteoclastic bone resorption and osteoblastic bone formation. Further studies on the doses of PTH and the durations of PTH exposure and withdrawal are required to determine a suitable regimen that induces more effective anabolic action of PTH on the bone structure. Since a recent study demonstrated that PTH predominantly affected preosteoblastic proliferation rather than osteoblastic bone synthesis, the effects of PTH-WD treatment on proliferation of preosteoblastic cells will be of particular interest for understanding the mechanism underlying such PTH treatment [27].

Acknowledgments We thank Dr. Toshinori Ishizuya for his instructive and helpful suggestions. This work was supported in part by a Grant-in-Aid for Scientific Research from the Japan Society for the Promotion of Science (14104015 to A.Y.) and by a grant from the Japanese Ministry of Education, Global Center of Excellence (GCOE) Program, "International Research Center for Molecular Science in Tooth and Bone Diseases."

References

1. Uzawa T, Hori M, Ejiri S, Ozawa H (1995) Comparison of the effects of intermittent and continuous administration of human parathyroid hormone (1–34) on rat bone. Bone 16:477–484
2. Iida-Klein A, Lu SS, Kapadia R, Burkhart M, Moreno A, Dempster DW, Lindsay R (2005) Short-term continuous infusion of human parathyroid hormone 1–34 fragment is catabolic with decreased trabecular connectivity density accompanied by hypercalcemia in C57BL/J6 mice. J Endocrinol 186:549–557
3. Dempster DW, Cosman F, Kurland ES, Zhou H, Nieves J, Woelfert L, Shane E, Plavetic K, Muller R, Bilezikian J, Lindsay R (2001) Effects of daily treatment with parathyroid hormone on bone microarchitecture and turnover in patients with osteoporosis: a paired biopsy study. J Bone Miner Res 16:1846–1853
4. Ejersted C, Andreassen TT, Oxlund H, Jorgensen PH, Bak B, Haggblad J, Torring O, Nilsson MH (1993) Human parathyroid hormone (1–34) and (1–84) increase the mechanical strength and thickness of cortical bone in rats. J Bone Miner Res 8:1097–1101
5. Dobnig H, Turner RT (1997) The effects of programmed administration of human parathyroid hormone fragment (1–34) on bone histomorphometry and serum chemistry in rats. Endocrinology 138:4607–4612
6. Hock JM, Gera I, Fonseca J, Raisz LG (1988) Human parathyroid hormone-(1–34) increases bone mass in ovariectomized and orchidectomized rats. Endocrinology 122:2899–2904
7. Riond JL, Goliat-von Fischer I, Kuffer B, Toromanoff A, Forrer R (1998) Influence of the dosing frequency of parathyroid hormone-(1–38) on its anabolic effect in bone and on the balance of calcium, phosphorus and magnesium. Z Ernahrungswiss 37:183–189
8. Neer RM, Arnaud CD, Zanchetta JR, Prince R, Gaich GA, Reginster JY, Hodsman AB, Eriksen EF, Ish-Shalom S, Genant HK, Wang O, Mitlak BH (2001) Effect of parathyroid hormone (1–34) on fractures and bone mineral density in postmenopausal women with osteoporosis. N Engl J Med 344:1434–1441
9. Taylor K, Gold DT, Miller P, Chen P, Wong M, Krohn K (2008) Teriparatide therapy in a community setting: persistence and use of other osteoporosis medications in DANCE. ASBMR meeting 2008 abstract 2008:Sa395
10. Kawase M, Tsuda M (1994) Vitamin D independent anabolic action of PTH in vivo. J Bone Miner Metab 12:S27–S31
11. Hoyer H, Perera G, Bernkop-Schnurch A (2010) Noninvasive delivery systems for peptides and proteins in osteoporosis therapy: a retroperspective. Drug Dev Ind Pharm 36:31–44
12. Ke HZ, Shen VW, Qi H, Crawford DT, Wu DD, Liang XG, Chidsey-Frink KL, Pirie CM, Simmons HA, Thompson DD (1998) Prostaglandin E2 increases bone strength in intact rats and in ovariectomized rats with established osteopenia. Bone 23:249–255
13. Parfitt AM, Drezner MK, Glorieux FH, Kanis JA, Malluche H, Meunier PJ, Ott SM, Recker RR (1987) Bone histomorphometry: standardization of nomenclature, symbols, and units. Report of the ASBMR Histomorphometry Nomenclature Committee. J Bone Miner Res 2:595–610
14. Frolik CA, Black EC, Cain RL, Satterwhite JH, Brown-Augsburger PL, Sato M, Hock JM (2003) Anabolic and catabolic bone effects of human parathyroid hormone (1–34) are predicted by duration of hormone exposure. Bone 33:372–379
15. Ishii H, Wada M, Furuya Y, Nagano N, Nemeth EF, Fox J (2000) Daily intermittent decreases in serum levels of parathyroid hormone have an anabolic-like action on the bones of uremic rats with low-turnover bone and osteomalacia. Bone 26:175–182
16. Lotinun S, Evans GL, Bronk JT, Bolander ME, Wronski TJ, Ritman EL, Turner RT (2004) Continuous parathyroid hormone induces cortical porosity in the rat: effects on bone turnover and mechanical properties. J Bone Miner Res 19:1165–1171
17. Cheng X, Li J, Lu Y, Keyak J, Lang T (2007) Proximal femoral density and geometry measurements by quantitative computed tomography: association with hip fracture. Bone 40:169–174
18. Ma YL, Cain RL, Halladay DL, Yang X, Zeng Q, Miles RR, Chandrasekhar S, Martin TJ, Onyia JE (2001) Catabolic effects of continuous human PTH (1–38) in vivo is associated with sustained stimulation of RANKL and inhibition of osteoprotegerin and gene-associated bone formation. Endocrinology 142:4047–4054
19. Li X, Qin L, Bergenstock M, Bevelock LM, Novack DV, Partridge NC (2007) Parathyroid hormone stimulates osteoblastic expression of MCP-1 to recruit and increase the fusion of pre/osteoclasts. J Biol Chem 282:33098–33106
20. Gold DT, Weinstein D, Pohl G, Chen Y, Krohn K, Meadows E (2009) Factors associated with discontinuation of teriparatide treatment: One-year results from the DANCE observational study addendum. ASBMR meeting 2009 abstract 2009:MO0357

21. Miller PD, Silverman SL, Gold DT, Taylor KA, Chen P, Wagman RB (2006) Rationale, objectives and design of the Direct Analysis of Nonvertebral Fracture in the Community Experience (DANCE) study. Osteoporos Int 17:85–90
22. Suzuki Y, Nagase Y, Iga K, Kawase M, Oka M, Yanai S, Matsumoto Y, Nakagawa S, Fukuda T, Adachi H, Higo N, Ogawa Y (2002) Prevention of bone loss in ovariectomized rats by pulsatile transdermal iontophoretic administration of human PTH(1–34). J Pharm Sci 91:350–361
23. Morley P (2005) Delivery of parathyroid hormone for the treatment of osteoporosis. Expert Opin Drug Deliv 2:993–1002
24. Black DM, Bouxsein ML, Palermo L, McGowan JA, Newitt DC, Rosen E, Majumdar S, Rosen CJ (2008) Randomized trial of once-weekly parathyroid hormone (1–84) on bone mineral density and remodeling. J Clin Endocrinol Metab 93:2166–2172
25. Horwitz MJ, Tedesco MB, Sereika SM, Syed MA, Garcia-Ocaña A, Bisello A, Hollis BW, Rosen CJ, Wysolmerski JJ, Dann P, Gundberg C, Stewart AF (2005) Continuous PTH and PTHrP infusion causes suppression of bone formation and discordant effects on 1, 25(OH)2 vitamin D. J Bone Miner Res 20:1792–1803
26. Katz I, Li M, Joffe I, Stein B, Jacobs T, Liang XG, Ke HZ, Jee W, Epstein S (1994) Influence of age on cyclosporin A-induced alterations in bone mineral metabolism in the rat in vivo. J Bone Miner Res 9:59–67
27. Luiz de Freitas PH, Li M, Ninomiya T, Nakamura M, Ubaidus S, Oda K, Udagawa N, Maeda T, Takagi R, Amizuka N (2009) Intermittent PTH administration stimulates pre-osteoblastic proliferation without leading to enhanced bone formation in osteoclast-less *c-fos*$^{-/-}$ mice. J Bone Miner Res 24:1586–1597

Human Pathology (2010) 41, 1718–1725

ELSEVIER

Human PATHOLOGY

www.elsevier.com/locate/humpath

Original contribution

Comprehensive keratin profiling reveals different histopathogenesis of keratocystic odontogenic tumor and orthokeratinized odontogenic cyst☆

Tadanobu Aragaki DDS[a,b], Yasuyuki Michi DDS, PhD[b], Ken-ichi Katsube MD, PhD[a], Narikazu Uzawa DDS, PhD[b], Norihiko Okada DDS, PhD[c], Takumi Akashi MD, PhD[d], Teruo Amagasa DDS, PhD[b], Akira Yamaguchi DDS, PhD[a], Kei Sakamoto DDS, PhD[a,*]

[a]*Section of Oral Pathology, Tokyo Medical and Dental University, Tokyo 113-0034, Japan*
[b]*Section of Maxillofacial Surgery, Tokyo Medical and Dental University, Tokyo 113-0034, Japan*
[c]*Section of Diagnostic Oral Pathology, Tokyo Medical and Dental University, Tokyo 113-0034, Japan*
[d]*Department of Pathology, Tokyo Medical and Dental University, Tokyo 113-0034, Japan*

Received 25 February 2010; revised 14 May 2010; accepted 14 May 2010

Keywords:
Keratocystic odontogenic tumor;
Orthokeratinized odontogenic cyst;
Keratin;
Gli2;
K17

Summary Keratocystic odontogenic tumor is a cystic lesion that behaves more aggressively than other jaw cysts. One of its characteristic histologic features is a parakeratinized uniform layer of lining epithelium. A jaw cyst lined with orthokeratinized epithelium is called an *orthokeratinized odontogenic cyst*. These keratinized jaw cysts are thought to be separate entities, although their histopathogenesis has not been fully assessed. To better understand these lesions, we performed comprehensive immunohistochemical profiling of the keratin expression of each. Orthokeratinized odontogenic cysts expressed keratin 1, keratin 2, keratin 10, and loricrin, suggesting differentiation toward normal epidermis. Keratocystic odontogenic tumors expressed keratin 4, keratin 13, keratin 17, and keratin 19, which is a unique expression pattern reminiscent of a mucosal squamous epithelium and an epithelial appendage. In neonatal rat tooth germ, cells strongly positive for keratin 17 and keratin 19 were observed, specifically in the dental lamina, implying the origin of keratocystic odontogenic tumor. GLI2, a downstream effector of hedgehog signaling, was significantly expressed in keratocystic odontogenic tumor and basal cell carcinoma, accompanied with robust expression of keratin 17, mammalian target of rapamycin, and BCL2. The expression of these GLI2- or keratin 17-related factors was not significantly observed in orthokeratinized odontogenic cysts. These findings provide evidence to support the viewpoint that keratocystic odontogenic tumor and orthokeratinized odontogenic cyst are separate entities, and furthermore suggest their characteristic histology, pathogenesis, and biological behaviors.

1. Introduction

Keratocystic odontogenic tumor (KCOT, also known as *odontogenic keratocyst*) is an intraosseous lesion that accounts for about 10% of jaw cysts [1]. Approximately 5% of KCOTs occur as multiple lesions, and a few of those cases occur as a

☆ This work was supported by a grant-in-aid from the Japanese Ministry of Education, Culture, Sports, Science, and Technology (Kakenhi 21592320), Tokyo, Japan.
* Corresponding author.
E-mail address: s-kei.mpa@tmd.ac.jp (K. Sakamoto).

0046-8177/$ – see front matter © 2010 Elsevier Inc. All rights reserved.
doi:10.1016/j.humpath.2010.05.007

manifestation of nevoid basal cell carcinoma syndrome (NBCCS) [2]. KCOT shows a characteristic histologic appearance. The cystic space is lined with a uniform parakeratinized squamous epithelium of 5 to 10 cell layers. The basal cells are aligned with vertically elongated nuclei. Mitotic activity is higher than other odontogenic cysts [3,4]. KCOT tends to recur after treatment; hence, a correct diagnosis is essential [1,5]. Several lines of evidence suggest that constitutive activation of hedgehog (Hh) signaling is a major causative factor for the development of KCOT and basal cell carcinoma (BCC), even in solitary cases [6-8]. Because of these features, it has been proposed that this cystic lesion should be regarded as a benign neoplasm [1,5,9]. About 10% of keratinizing jaw cysts are lined predominantly by orthokeratinized epithelium, and this variant is called *orthokeratinized odontogenic cyst* (OOC) [10]. OOC exhibits a less aggressive behavior with a low recurrence rate [11]. It is generally accepted that OOC should be regarded as a separate entity from KCOT [9]. However, the diagnostic criteria are yet descriptive; and the biological properties of these lesions have not been fully assessed. Therefore, the rationale for their separation, which is mainly based on the mode of keratinization, should be further evaluated.

Keratin is an epithelial-specific intermediate filament protein whose production is the primary function of squamous cells. Keratin has many subtypes: the human genome contains 37 functional epithelial keratin genes. Among them, keratins from keratin 1 (K1) to K20 are major subtypes that are expressed in considerable amounts. These subtypes can be divided into basic (K1-K8) and acidic (K9-K20) ones; both types are coexpressed, dimerize together, and form a cytoskeleton to maintain the cell shape and the integrity of the epithelium. The expression is regulated so that specific sets of keratins are produced depending on cell type and differentiation state. For example, a glandular epithelium typically expresses keratins of a low molecular weight such as K7, K8, K18, and K19; and a squamous epithelium of skin expresses K1, K2, and K10 as well as loricrin (LOR), whereas a squamous epithelium of mucosa expresses K4 and K13. Therefore, the evaluation of the keratin expression profile can facilitate cell typing and identification [12].

Because the property of a cell greatly depends on its lineage and differentiation state, keratin profiling of KCOT and OOC would provide essential information for understanding the pathogenesis and the biological behavior of these diseases. Although previous reports described expression of some individual keratins in these lesions [13-16], the comprehensive keratin profiles and their pathologic significance are yet to be elucidated.

In this study, we examine the expression of all the major keratins in KCOT and OOC. The comparison of profiles reveals keratins that characterize KCOT and OOC and that explain their histology, further suggesting their pathogenesis and biological behaviors.

2. Materials and methods

2.1. Tissue specimens

Surgical specimens resected in the Hospital of Tokyo Medical and Dental University were collected. The pathologic diagnoses were KCOT (20), OOC (20), dentigerous cyst (10), epidermoid cyst (10), ameloblastoma (7), and BCC (6). The clinical data of KCOT and OOC cases are summarized in Table 1. Six cases of KCOT occurred as multiple lesions. The

Table 1 Summarized clinical data of KCOT and OOC

	Age/sex	Size	Location		Age/sex	Size	Location
KCOT1	29/F	30 × 30	Mandible	OOC1	21/F	NA	Mandible
KCOT2	14/F	15 × 21	Mandible	OOC2	22/M	25 × 32	Mandible
KCOT3	15/F	16 × 12	Mandible	OOC3	22/M	30 × 35	Mandible
KCOT4	19/M	NA	Mandible	OOC4	26/F	NA	Mandible
KCOT5	21/M	27 × 21	Maxilla	OOC5	27/F	40 × 40	Maxilla
KCOT6	34/F	36 × 30	Mandible	OOC6	27/F	NA	Mandible
KCOT7	51/F	NA	Maxilla	OOC7	28/F	18 × 17	Mandible
KCOT8	56/M	12 × 20	Mandible	OOC8	28/M	30 × 15	Mandible
KCOT9	21/F	15 × 20	Mandible	OOC9	28/F	25 × 30	Maxilla
KCOT10	59/M	19 × 10	Mandible	OOC1O	29/F	NA	Mandible
KCOT11	65/M	NA	Mandible	OOC11	35/M	NA	Mandible
KCOT12	65/M	13 × 12	Mandible	OOC12	39/M	30 × 25	Mandible
KCOT13	72/M	NA	Mandible	OOC13	40/M	34 × 20	Mandible
KCOT14	19/F	21 × 16	Mandible	OOC14	41/M	40 × 30	Maxilla
KCOT15	33/M	Max 45 × 15	Multiple (3)	OOC15	41/M	NA	Maxilla
KCOT16	10/M	Max 27 × 29	Multiple (3)	OOC16	51/M	NA	Mandible
KCOT17	13/F	Max 30 × 22	Multiple (2)	OOC17	60/M	NA	Mandible
KCOT18	17/F	NA	Multiple (5)	OOC18	64/M	NA	Mandible
KCOT19	13/F	NA	Multiple (4)	OOC19	68/M	30 × 20	Mandible
KCOT20	11/F	Max 37 × 33	Multiple (5)	OOC20	11/M	50 × 25	Maxilla

tissue specimens were fixed in 10% buffered formalin and embedded in paraffin. A neonatal rat (F344/Jcl) was killed and was fixed in 4% paraformaldehyde/phosphate-buffered saline for 2 days, decalcified in 10% EDTA for 1 week, dehydrated, and embedded in paraffin. The experimental procedures were approved by the university ethics committee.

2.2. Immunohistochemical staining

Immunohistochemical staining was performed according to the standard protocol. For antigen retrieval, the sections were placed in TE buffer (10 mmol/L Tris [pH = 9.0], 1 mmol/L EDTA) and autoclaved at 120°C for 20 minutes. The antibodies used in this study are listed in Table 2. The dilution factors for all primary antibodies were 1:500. The sensitivities and specificities of these antibodies were confirmed in a pilot experiment using specimens of normal skin, tongue, salivary gland, and digestive tract as a reference tissue. For incubation with anti-Gli2 antibody, Can Get Signal (Toyobo, Osaka, Japan) was used. EnVision Dual Link (Dako, Glostrup, Denmark) or ImmPRESS Anti-Goat Ig Kit (Vector Laboratories, Burlingame, CA) was used as the secondary antibody.

Table 2 Antibodies used in this study

Antigen	Supplier	Clone name
K1	Santa Cruz Biotechnology (Santa Cruz, CA)	N-20
K2	Progen (Heidelberg, Germany)	Ks2.342.7.1
K4	Epitomics (Burlingame, CA)	EP1599Y
K5	Monosan (Uden, Netherlands)	XM26
K6	Thermo Fisher Scientific (Fremont, CA)	LHK6B
K7	Dako (Glostrup, Denmark)	RN7
K8	Leica Microsystems (Wetzlar, Germany)	TS1
K9	Euro-Diagnostica (Malmö, Sweden)	Ks9.70/ Ks9.216
K10	Thermo Fisher Scientific (Fremont, CA)	DE-K10
K13	Leica Microsystems (Wetzlar, Germany)	KS-1A3
K14	Abcam (Cambridge, MA)	LL002
K15	Epitomics (Burlingame, CA)	EPR1614Y
K16	Thermo Fisher Scientific (Fremont, CA)	LL025
K17	Dako (Glostrup, Denmark)	E3
K18	Dako (Glostrup, Denmark)	DC10
K19	Epitomics (Burlingame, CA)	EPR1579Y
K20	Dako (Glostrup, Denmark)	PW1
Hair keratin	Santa Cruz Biotechnology (Santa Cruz, CA)	AE13
LOR	Covance Research Products (Denver, PA)	PRB-145P
BCL2	Dako (Glostrup, Denmark)	clone124
GLI2	Santa Cruz Biotechnology (Santa Cruz, CA)	H-300
mTOR/ FRAP	Epitomics (Burlingame, CA)	Y391

3. Results

3.1. Keratin profiles of KCOT and OOC are distinctive

The immunohistochemical staining results of representative cases of KCOT and OOC are shown in Fig. 1. The expression was evaluated at the site without inflammation to avoid misinterpretation due to reactive changes. The keratin profiles of KCOT and OOC are summarized and depicted by a schematic illustration (Fig. 2). The most relevant keratins for distinguishing KCOT from OOC were K4, K13, K17, and K19, which were consistently and strongly positive in KCOT and almost negative in OOC, and K1, K10, and LOR, which were consistently positive in OOC and negative in KCOT. In KCOT, K17 and K19 were expressed in both the basal and suprabasal cells, whereas K4 and K13 were expressed in the superficial layer. In OOC, K1 and K10 were expressed in the suprabasal cells; and LOR was expressed superficially. Expression of several keratin subtypes exhibited case-dependent variations, (for example, K8 and K18 expression was observed in some cases of KCOT [Supplementary Figure S1]), but no apparent subgroup defined by the keratin profile was noted. No significant difference was observed in the keratin profiles between solitary KCOT and multiple KCOT (data not shown). These results indicated that KCOT and OOC expressed unique sets of keratin subtypes, suggesting that each constitutes a distinct entity defined by the keratin profile.

3.2. The keratin profile of OOC is almost identical to that of the epidermis

For better understanding of the origin and the biological properties of a tumor, it is informative to identify the normal tissue whose differentiation state resembles that of the tumor cells. We searched for a tissue that exhibited the keratin profile similar to KCOT and OOC. The keratin profile of OOC was almost identical to that of epidermis, whose basal cells were positive for K5, K14, and K15 and whose suprabasal cells were strongly positive for K1, K2, and K10 with superficial LOR expression (data not shown). K4(+)K13(+) phenotype was seen in the nonkeratinized squamous epithelium such as that of oral or esophageal mucosa, and K17(+)K19(+) phenotype was seen in epithelial appendages such as hair follicles; but the K4(+)K13(+)K17(+)K19(+) phenotype of KCOT was unique and was different from any normal adult tissues.

3.3. The keratin profile of KCOT is similar to that of the dental lamina

We extended the examination of keratin expression to neonatal oral tissue including tooth germ. Because of the

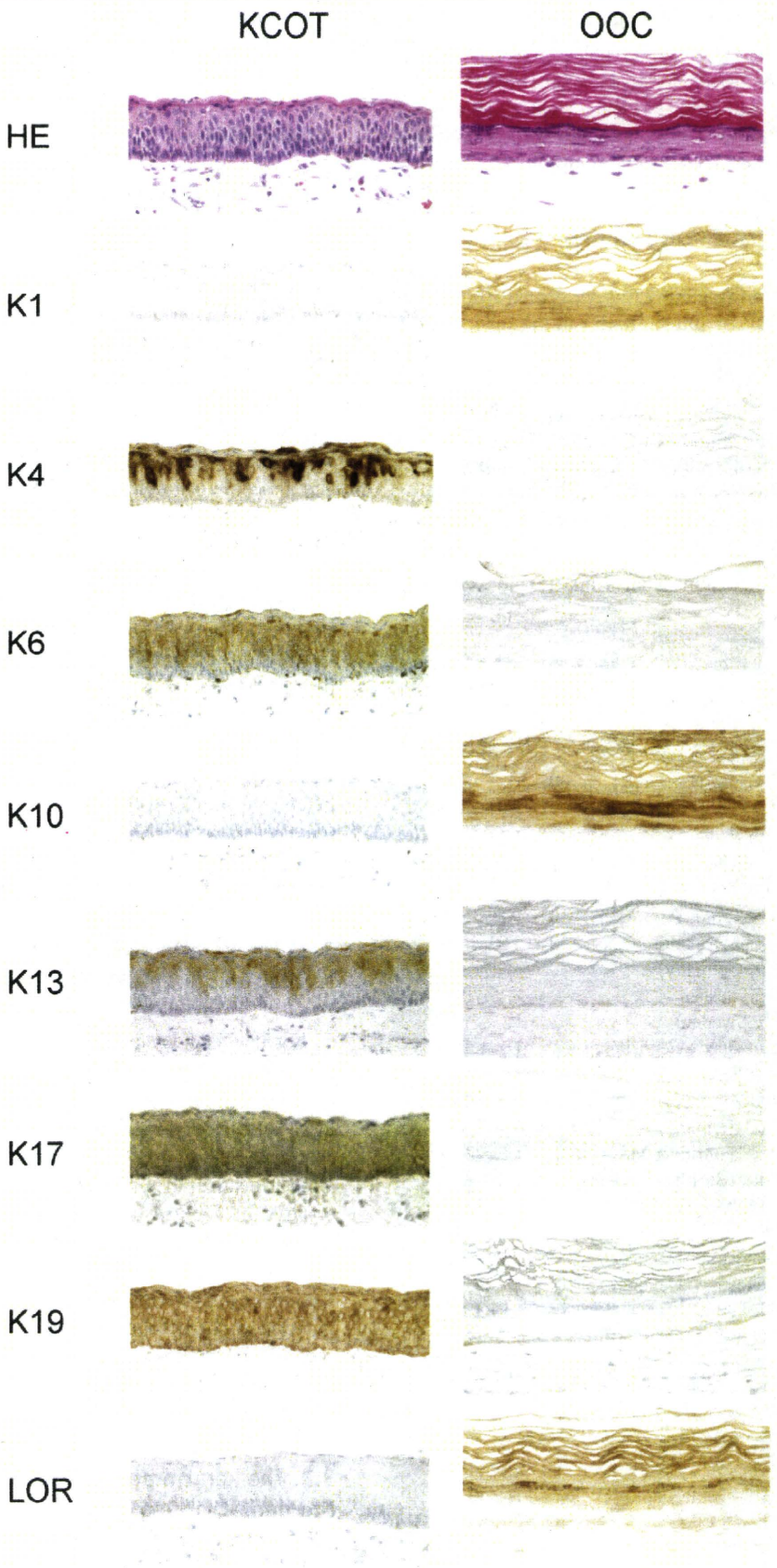

Fig. 1 Immunohistochemical expression of various keratins and LOR in representative cases of KCOT and OOC (original magnification, x100).

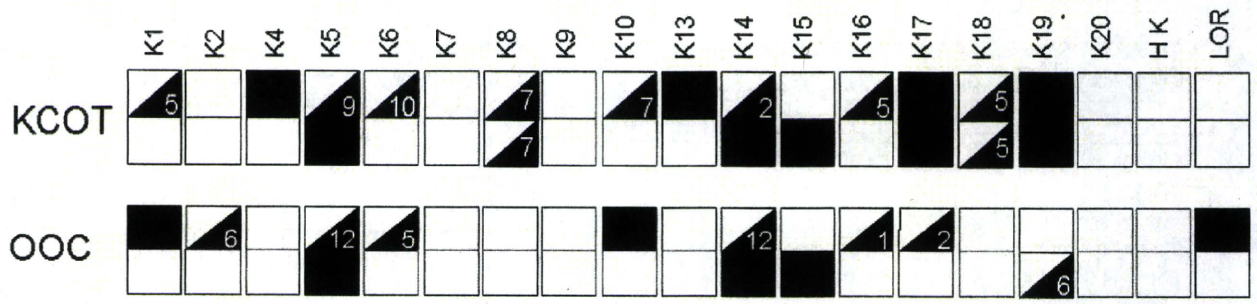

Fig. 2 Schematically illustrated keratin expression profiles of KCOT and OOC. The epithelium is divided into 2 compartments: the basal (lower box) and the suprabasal compartments (upper box), and the expression is represented by a 3-grade evaluation. The black shading represents that the expression was observed in virtually all the cells of all the cases examined. The white shading represents that the expression was almost completely negative in all the cases. The diagonal represents that the expression is partially positive in some cases, with a number of positive cases. Abbreviation: HK, hair keratins.

difficulty of obtaining a human tissue, a neonatal rat was used. In the neonatal tooth germ, the cells with distinct K17(+)K19 (+) phenotype were observed in the dental lamina, whereas the other part of the tooth germ and the oral epithelium expressed only a trace of these keratins (Fig. 3, Table 3).

3.4. Keratin profiles of other cystic lesions

We examined the keratin profile in other cystic lesions that are considered in the differential diagnosis of KCOT and OOC. Data for the relevant keratin expressions are summarized in Table 3. The keratin profile of dentigerous cyst was different from that of KCOT in its absence of K17 expression. Cystic type ameloblastoma showed a keratin profile similar to that of KCOT; but the expression of K17 was superficial, contrasting with the diffuse expression in KCOT (Table 3, Supplementary Figure S2). Epidermoid cyst showed an almost identical keratin profile to OOC.

3.5. Expression of GLI2 and mammalian target of rapamycin is associated with K17 expression in KCOT

Because these results suggested the significance of K17 in the pathogenesis of these lesions, we examined the expression of K17-related factors in KCOT, OOC, and BCC. GLI2, a downstream effector of Hh signaling and an inducer of K17 expression, was significantly up-regulated in the tumor cells of all 6 BCC cases and was strongly expressed in all cases of KCOT, exhibiting nuclear localization (Fig. 4). Keratins considerably expressed in BCC were only K17 as well as basal cell keratins K5, K14, and K15; and thus, K17 was consistently coexpressed with GLI2 in both BCC and KCOT. Mammalian target of rapamycin (mTOR), which is an essential regulator of cell growth and is activated by K17 expression, was robustly expressed in BCC and KCOT. In contrast to KCOT, which showed diffuse strong expression of mTOR, the expression in OOC was largely restricted to the basal cells (Fig. 4). Antiapoptotic protein BCL2 was also strongly expressed in BCC and KCOT. OOC was almost negative for GLI2 and BCL2, as well as for K17.

4. Discussion

K4 and K13 are differentiation-related keratin pairs that are predominantly expressed only in the suprabasal layer of nonkeratinized squamous epithelium (Supplementary Figure S3). The superficial cells strongly positive for K4 and K13 in KCOT were mostly parakeratinized; therefore, their expression in KCOT appeared to associate with parakeratinization characteristically observed in this lesion. Similarly, K1 and K10 are specific for the suprabasal

Fig. 3 Immunohistochemical expression of K17 and K19 in the first molar tooth germ of a neonatal rat. Cells strongly positive for K17 and K19 were observed in the dental lamina (arrow).

Table 3 Summarized expression of relevant keratins in various tissues and lesions

	K17	K19
KCOT	++	++
OOC	−	−
Inner ameloblast	−	−
Outer ameloblast	+	−
Stellate reticulum	−	−
Dental lamina	++	++
Dentigerous cyst	−	++
Cystic ameloblastoma	+	++

cells of keratinized squamous epithelium and appeared to associate with orthokeratinization in OOC. Typically, the expressions of the K4/K13 pair and the K1/K10 pair are mutually exclusive of each other; and the mode of keratinization, which is one of the major histologic features separating KCOT and OOC, is thus due to the selection of these 2 pairs of keratin subtypes. OOC also expressed K2 and LOR, which are expressed in the upper spinous cell layer and in the cornified envelope, respectively. These results indicated that the differentiation of OOC cells as epidermis is almost complete, which may associate with the unaggressive behavior of OOC. In contrast, KCOT showed a unique and unusual keratin profile, suggesting dysregulation of differentiation.

K8 and K18 are the most primitive forms among keratin families, and their expression starts as early as in ectoderm [12]; both are typically expressed in a simple epithelium, but not in a squamous epithelium. Occasional expression of K8 and K18 in KCOT suggests that the lesion may arise from

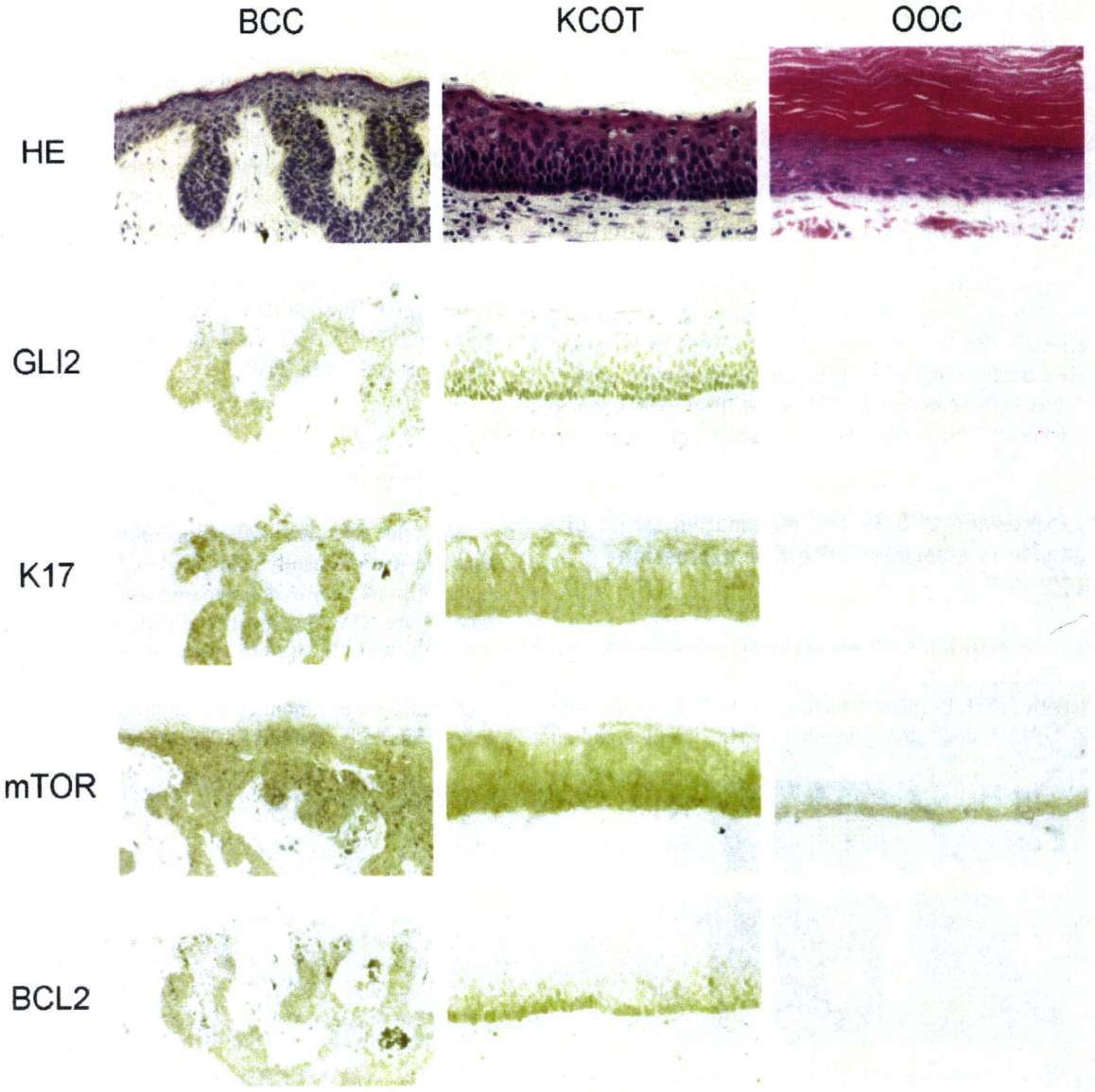

Fig. 4 Immunohistochemical expression of GLI2, K17, mTOR, and BCL2 in BCC, KCOT, and OOC.

cells that retain primitive properties, as is seen in embryonic epithelium. In a single-layered simple epithelium, keratin filaments (composed of K8, K18, and K19) distribute with apical polarization, contrasting with a squamous epithelium whose keratin filaments show basoapically uniform distribution. The significance of the asymmetric distribution of keratin filaments is yet poorly understood, but it has been suggested that these keratins participate in the generation of epithelial cell polarity [17]. Abundant expression of K19 may associate with generation of a polarized, vertically elongated cell shape observed in KCOT.

K6, K16, and K17 are related to regeneration; and they are induced in a hyperproliferative epithelium after injury [12,18]. Among these, K17 was consistently and strongly expressed in KCOT. K17 increases mTOR signaling activity, stimulating protein synthesis and cell growth [19]. Robust expression of K17 and concomitant up-regulation of mTOR in KCOT may associate with its proliferative and aggressive behavior.

Strong expression of K17 and K19 was distinct from normal squamous epithelium and seemed a unique feature of KCOT. Interestingly, cells strongly positive for K17 and K19 were observed exclusively in a dental lamina of a late-stage tooth germ. This seemed to support the notion that KCOT arises from the remnant of dental lamina cells.

A striking similarity of the keratin profile was observed also between KCOT and the hair follicle bulge, which expressed both K17 and K19. Although the bulge expresses various hair keratins instead of K4 and K13, the keratin profile of the bulge cells is identical to the basal cells of KCOT, which are positive for K5, K14, K15, K17, and K19. Considering the analogous histogenesis between tooth germ and hair follicle development, this similarity provides an implication for the pathogenesis of KCOT.

NBCCS is an autosomal dominant genetic disease that exhibits multiple KCOT and BCC. NBCCS is typically caused by a mutation in the Hh receptor *PATCHED* gene, which leads to constitutive active Hh signaling [8]. BCC is thought to arise from pluripotent hair follicle cells [20], and the Hh signaling is essential not only for the occurrence of BCC but also for hair follicle development [21]. Aberrant Hh signaling may also associate with nonsyndromic KCOT and BCC [7,8]; and in fact, we demonstrated that the effector of Hh signaling GLI2 was significantly expressed in both KCOT and BCC, accompanied with up-regulation of K17 that is a putative downstream target of Hh signaling [22]. These results suggest that GLI2 up-regulation, either or not by aberrant Hh signaling, is one of the direct causes of KCOT development.

K5-Gli2 transgenic mice develop jaw cysts derived from epithelial rests of Malassez [23]. These cysts show histologic features of OOC, but not of KCOT. This animal experiment implied that GLI2 is important also for OOC development. However, GLI2 expression was not detected in human OOC, leaving the origin and pathogenesis of OOC yet to be elucidated.

We found that the antiapoptotic protein BCL2 was up-regulated in KCOT. Because BCL2 has been shown to be a direct transcriptional target of GLI2 [24], the GLI2-BCL2 cascade may play a role in KCOT development, possibly by impaired apoptosis to correct secondary mutation events.

In conclusion, keratin profiling indicates that the differentiation states of KCOT and OOC are distinct and completely different from each other. The repertoire of the expressed keratin subtypes seems to associate with their characteristic histology and further suggests their pathogenesis and biological behaviors.

Appendix A. Supplementary data

Supplementary data associated with this article can be found, in the online version, at doi:10.1016/j.humpath.2010.05.007.

References

[1] Gnepp DR. Diagnostic surgical pathology of the head and neck. 2nd ed. Philadelpia, PA: Saunders; 2009.
[2] Gonzalez-Alva P, Tanaka A, Oku Y, et al. Keratocystic odontogenic tumor: a retrospective study of 183 cases. J Oral Sci 2008;50:205-12.
[3] Shear M. The aggressive nature of the odontogenic keratocyst: is it a benign cystic neoplasm? Part 2. Proliferation and genetic studies. Oral Oncol 2002;38:323-31.
[4] Kolar Z, Geierova M, Bouchal J, Pazdera J, Zboril V, Tvrdy P. Immunohistochemical analysis of the biological potential of odontogenic keratocysts. J Oral Pathol Med 2006;35:75-80.
[5] Madras J, Lapointe H. Keratocystic odontogenic tumour: reclassification of the odontogenic keratocyst from cyst to tumour. J Can Dent Assoc 2008;74:165-165h.
[6] Ohki K, Kumamoto H, Ichinohasama R, Sato T, Takahashi N, Ooya K. PTC gene mutations and expression of SHH, PTC, SMO, and GLI-1 in odontogenic keratocysts. Int J Oral Maxillofac Surg 2004; 33:584-92.
[7] Sun LS, Li XF, Li TJ. PTCH1 and SMO gene alterations in keratocystic odontogenic tumors. J Dent Res 2008;87:575-9.
[8] Zedan W, Robinson PA, Markham AF, High AS. Expression of the sonic hedgehog receptor "PATCHED" in basal cell carcinomas and odontogenic keratocysts. J Pathol 2001;194:473-7.
[9] Barnes L, Eveson JW, Reichart P, Sidransky D. Pathology and Genetics of Head and Neck Tumours. IARC WHO Classification of Tumours. No 9. IARC, Lyon, France: 2005.
[10] Li TJ, Kitano M, Chen XM, et al. Orthokeratinized odontogenic cyst: a clinicopathological and immunocytochemical study of 15 cases. Histopathology 1998;32:242-51.
[11] Wright JM. The odontogenic keratocyst: orthokeratinized variant. Oral Surg Oral Med Oral Pathol 1981;51:609-18.
[12] Moll R, Divo M, Langbein L. The human keratins: biology and pathology. Histochem Cell Biol 2008;129:705-33.
[13] Shear M. The aggressive nature of the odontogenic keratocyst: is it a benign cystic neoplasm? Part 3. Immunocytochemistry of cytokeratin and other epithelial cell markers. Oral Oncol 2002;38:407-15.
[14] Stoll C, Stollenwerk C, Riediger D, Mittermayer C, Alfer J. Cytokeratin expression patterns for distinction of odontogenic keratocysts from dentigerous and radicular cysts. J Oral Pathol Med 2005;34:558-64.

[15] Vuhahula E, Nikai H, Ijuhin N, et al. Jaw cysts with orthokeratinization: analysis of 12 cases. J Oral Pathol Med 1993;22:35-40.
[16] Dos Santos JN, Oliveira GQ, Gurgel CA, et al. Altered expression of cytokeratins in primary, recurrent and syndrome keratocystic odontogenic tumors. J Mol Histol 2009.
[17] Oriolo AS, Wald FA, Ramsauer VP, Salas PJ. Intermediate filaments: a role in epithelial polarity. Exp Cell Res 2007;313:2255-64.
[18] McGowan K, Coulombe PA. The wound repair-associated keratins 6, 16, and 17. Insights into the role of intermediate filaments in specifying keratinocyte cytoarchitecture. Subcell Biochem 1998;31: 173-204.
[19] Kim S, Wong P, Coulombe PA. A keratin cytoskeletal protein regulates protein synthesis and epithelial cell growth. Nature 2006; 441:362-5.
[20] Yang SH, Andl T, Grachtchouk V, et al. Pathological responses to oncogenic hedgehog signaling in skin are dependent on canonical Wnt/beta3-catenin signaling. Nat Genet 2008;40:1130-5.
[21] Grachtchouk M, Mo R, Yu S, et al. Basal cell carcinomas in mice overexpressing Gli2 in skin. Nat Genet 2000;24:216-7.
[22] Bianchi N, Depianto D, McGowan K, Gu C, Coulombe PA. Exploiting the keratin 17 gene promoter to visualize live cells in epithelial appendages of mice. Mol Cell Biol 2005;25:7249-59.
[23] Grachtchouk M, Liu J, Wang A, et al. Odontogenic keratocysts arise from quiescent epithelial rests and are associated with deregulated hedgehog signaling in mice and humans. Am J Pathol 2006;169:806-14.
[24] Regl G, Kasper M, Schnidar H, et al. Activation of the BCL2 promoter in response to Hedgehog/GLI signal transduction is predominantly mediated by GLI2. Cancer Res 2004;64:7724-31.

Biochemical and Biophysical Research Communications 405 (2011) 455–461

Contents lists available at ScienceDirect

Biochemical and Biophysical Research Communications

journal homepage: www.elsevier.com/locate/ybbrc

The regulation of tooth morphogenesis is associated with epithelial cell proliferation and the expression of *Sonic hedgehog* through epithelial–mesenchymal interactions

Kentaro Ishida [a], Mayumi Murofushi [a], Kazuhisa Nakao [b], Ritsuko Morita [b], Miho Ogawa [b,c], Takashi Tsuji [a,b,c,*]

[a] Faculty of Industrial Science and Technology, Tokyo University of Science, Chiba 278-8510, Japan
[b] Research Institute for Science and Technology, Tokyo University of Science, Chiba 278-8510, Japan
[c] Organ Technologies Inc., Tokyo 101-0048, Japan

ARTICLE INFO

Article history:
Received 25 December 2010
Available online 19 January 2011

Keywords:
Tooth morphogenesis
Organ germ method
Sonic hedgehog
Epithelial–mesenchymal interaction

ABSTRACT

Ectodermal organs, such as the tooth, salivary gland, hair, and mammary gland, develop through reciprocal epithelial–mesenchymal interactions. Tooth morphologies are defined by the crown width and tooth length (macro-morphologies), and by the number and locations of the cusp and roots (micro-morphologies). In our current study, we report that the crown width of a bioengineered molar tooth, which was reconstructed using dissociated epithelial and mesenchymal cells via an organ germ method, can be regulated by the contact area between epithelial and mesenchymal cell layers. We further show that this is associated with cell proliferation and *Sonic hedgehog* (*Shh*) expression in the inner enamel epithelium after the germ stage has formed a secondary enamel knot. We also demonstrate that the cusp number is significantly correlated with the crown width of the bioengineered tooth. These findings suggest that the tooth micro-morphology, i.e. the cusp formation, is regulated after the tooth width, or macro-morphology, is determined. These findings also suggest that the spatiotemporal patterning of cell proliferation and the *Shh* expression areas in the epithelium regulate the crown width and cusp formation of the developing tooth.

1. Introduction

All organs arise from their respective germs through reciprocal interactions between the epithelium and mesenchyme during organogenesis in the developing embryo [1–4]. Organs develop according to predetermined programs, which include the regulation of their location, cell number and morphology. The induction of organ development at the appropriate future location requires both regional and genetic specificity [5]. It is well known in this regard that many cytokines, such as the fibroblast growth factor (FGF), hedgehog, Wnt, and transforming growth factor (TGF)/bone morphogenetic protein (BMP) families, play essential roles in epithelial and mesenchymal interactions during organogenesis [1,2].

Ectodermal organs, such as the tooth, salivary gland, hair, and mammary gland, also develop through reciprocal epithelial and mesenchymal interactions [1,2]. The number and morphology of the teeth in the tooth forming field, which are specified by the expression of homeobox genes in the underlying neural crest-derived mesenchyme in the embryonic jaw, have previously been determined during developmental process [3]. Tooth development begins with epithelium thickening and innervation of the underling mesenchyme [1,2]. At the dental placode stage, the dental epithelium induces the condensation of the surrounding mesenchymal cells through the expression of signaling molecule genes such as *Shh*, *Fgf8*, *Bmp4* and *Wnt10b*, which can induce the expression of a large number of transcription factors such as *Msx1*, *Pax9* and *Gli* in the mesenchyme [2]. These interactions between these signaling molecules and transcription factors induce the formation of an enamel knot, which acts as a signaling center to coordinate tooth germ development [2]. *Shh* plays a particularly important role in tooth germ induction and formation, including the primary enamel knot formation, and thereafter functions in the growth and differentiation of epithelial cells into the ameloblast [6].

Following tooth germ formation, the epithelial and mesenchymal cells in the tooth germ differentiate into tooth-tissue forming cells and secrete hard tissues such as enamel dentin, cementum, and alveolar bone [7]. The tooth types that result, such as incisors (monocuspid) and molars (multicuspid), are thought to be

* Corresponding author at: Department of Biological Science and Technology, Faculty of Industrial Science and Technology, Tokyo University of Science, Noda, Chiba 278-8510, Japan. Fax: +81 4 7122 1499.
E-mail addresses: t-tsuji@rs.noda.tus.ac.jp, t-tsuji@nifty.com (T. Tsuji).

0006-291X/$ - see front matter © 2011 Elsevier Inc. All rights reserved.
doi:10.1016/j.bbrc.2011.01.052

regulated by regional gene expression which controls the tooth-forming region at the mesenchyme during embryonic development [3]. It has also been reported that the tooth type and morphology is determined by the balance of endogenous inhibitors and mesenchymal activator [8] and by regulatory mechanisms that operate in the tooth forming field [9]. Tooth morphology is defined by both the crown size and tooth length at the macro-morphology, and by the number and position of the cusp and roots at the micro-morphology [10]. Although the crown size, as a determinant of macro-patterning during tooth morphogenesis, is based on the reaction-diffusion model [10], the underlying molecular and cellular mechanisms, such as cell growth and cell movement, have remained unexplored. The regulation of the cusp number and position, which underlies the micro-patterning of the tooth, is thought to be closely involved in the formation of the secondary enamel knot. This is regulated spatiotemporally by the reciprocal activation and inhibition of cell proliferation in the epithelium and mesenchyme via the reaction-diffusion mechanism, and determines the cusp pattern formation through cell growth and movement [11,12]. However, it remains to be undetermined how the regulation of cell proliferation and the underlying molecular mechanisms are involved in crown size determination through epithelial–mesenchymal interactions.

In our current study, we analyzed the mechanisms that determine the crown width and cusp number of a bioengineered tooth via the regulation of the contact area between the epithelial and mesenchymal cell layers. We provide evidence to suggest that the spatiotemporal regulation of epithelial cell proliferation and *Shh* expression in the tooth germ-epithelium is involved in determining the crown and cusp morphologies during tooth development.

2. Materials and methods

2.1. Animals

C57BL/6 mice were purchased from SLC Inc., (Shizuoka, Japan). B6.Cg-*Shh*$^{tm1(EGFP/cre)Cjt}$/J mice were obtained from The Jackson Laboratory (Bar Harbor, ME). All mouse care and handling complied with the NIH guidelines for animal research and all experimental protocols involving animals were approved by the Tokyo University of Science Animal Care and Use Committee.

2.2. Reconstitution of a bioengineered tooth germ from single cells

Molar tooth germs were dissected from the mandibles of ED14.5 mice in order to reconstitute a bioengineered tooth germ by a three-dimensional cell manipulation method, the previously described organ germ method [13]. To regulate the contact length between the epithelial and mesenchymal cell layers, the epithelial and mesenchymal columnar cell layers were arranged contiguously using a micro-syringe with a 0.330 μm inner diameter to inject both cell types into a 30 μm gel drop of Cellmatrix type I-A (Nitta gelatin, Osaka, Japan). The contact length between epithelial and mesenchymal cell layers was then measured using Axioobserver (Carl Zeiss, Jena, Germany) with an AxioCAM MRc5 (Carl Zeiss) microscope and Axiovision software (Carl Zeiss). The resulting bioengineered tooth germs were incubated at 37 °C for 2–7 days as described previously [13].

2.3. Microcomputed tomography (Micro-CT) measurements

Radiographic imaging was performed using X-rays and a Micro-CT device (R_mCT, Rigaku) with exposures set at 90 kV and 150 mA. Micro CT images were captured using i-view R (Morita) and Imaris (Carl Zeiss).

2.4. Histochemical and immunohistochemical analysis

Histochemical tissue analyses were performed as described previously [13]. Briefly, tissue sections (10 μm) were stained with hematoxylin and eosin and observed using Axioimager A1 (Carl Zeiss) with an AxioCAM MRc5 (Carl Zeiss) microscope. Tissues were prepared for immunohistochemistry as described previously [14]. For fluorescent immunohistochemistry, the tissue sections (10 μm) were incubated with an anti-Ki67 primary antibody (1:100; Abcam, Cambridge, MA) and Hoechst33342 (1:500; Invitrogen, Carlsbad, CA) for 2 h at room temperature. Immunoreactivity was detected using an Alexa Fluor® 594-conjugated Goat Anti-rabbit IgG secondary antibody (1:500, Invitrogen). Fluorescence microscopy images were captured under a confocal microscope (LSM 510; Carl Zeiss) and processed with AxioVision software (Carl Zeiss).

2.5. In situ hybridization

In situ hybridizations were performed using 10 μm frozen sections as described previously [13]. Digoxygenin-labeled probes for specific transcripts were prepared by PCR with primers designed using published sequences (*Shh*; GenBank ID: NM_009170, *Fgf4*; GenBank ID: NM_010202, *Fgf3*; GenBank ID: NM_008007).

2.6. Statistical analysis

Statistically-significant differences were determined by the unpaired student's *t*-test. The analysis was performed using the Common Gateway Interface Program (twk, Saint John's University).

3. Results

3.1. The crown width of a bioengineered tooth correlates with the length of the contact area between the epithelial and mesenchymal cell layers

We first investigated whether the contact area between the epithelial and mesenchymal cell layers affect the eventual morphology, such as the crown width and cusp number, of a bioengineered tooth germ reconstituted from ED14.5 molar tooth germ-derived single cells using the organ germ method [13]. The bioengineered tooth germs, which were prepared using various contact lengths between the epithelial and mesenchymal cell layers, were reconstructed with a micro-syringe of a 0.330 μm inner diameter (Fig. 1A). After one day of *in vitro* organ culture, we classified the bioengineered tooth germs into three-groups by measuring the contact length using a side-view as follows: short-contact length (short), up to 450 μm; middle-contact length (middle), 450–900 μm, and long-contact length (long), 900–1500 μm. The mean widths were also calculated as follows: short, 366 ± 103 μm; middle, 584 ± 103 μm; and long, 934 ± 239 μm. All of the bioengineered tooth germs reached the early bell developmental stage at the same time as a natural tooth germ following 3–5 days in culture (Fig. 1B). To examine the correlation between the contact length and the tooth crown width of the bioengineered teeth, the germs were transplanted into a subrenal capsule. At 21 days post-transplantation, the entire bioengineered tooth germ developed into a tooth unit with the correct structure comprising enamel, ameloblast, dentin, odontoblast, dental pulp, alveolar bone, and blood vessels (Fig. 1C). Typical images of these teeth classified into the three-groups above are shown in Fig. 1C. The mean crown widths of the bioengineered molars that developed from the short, middle and long germ groups were 497 ± 118 μm, 727 ± 271 μm, and 1073 ± 186 μm, respectively. All of the crown widths of the samples following subrenal capsule

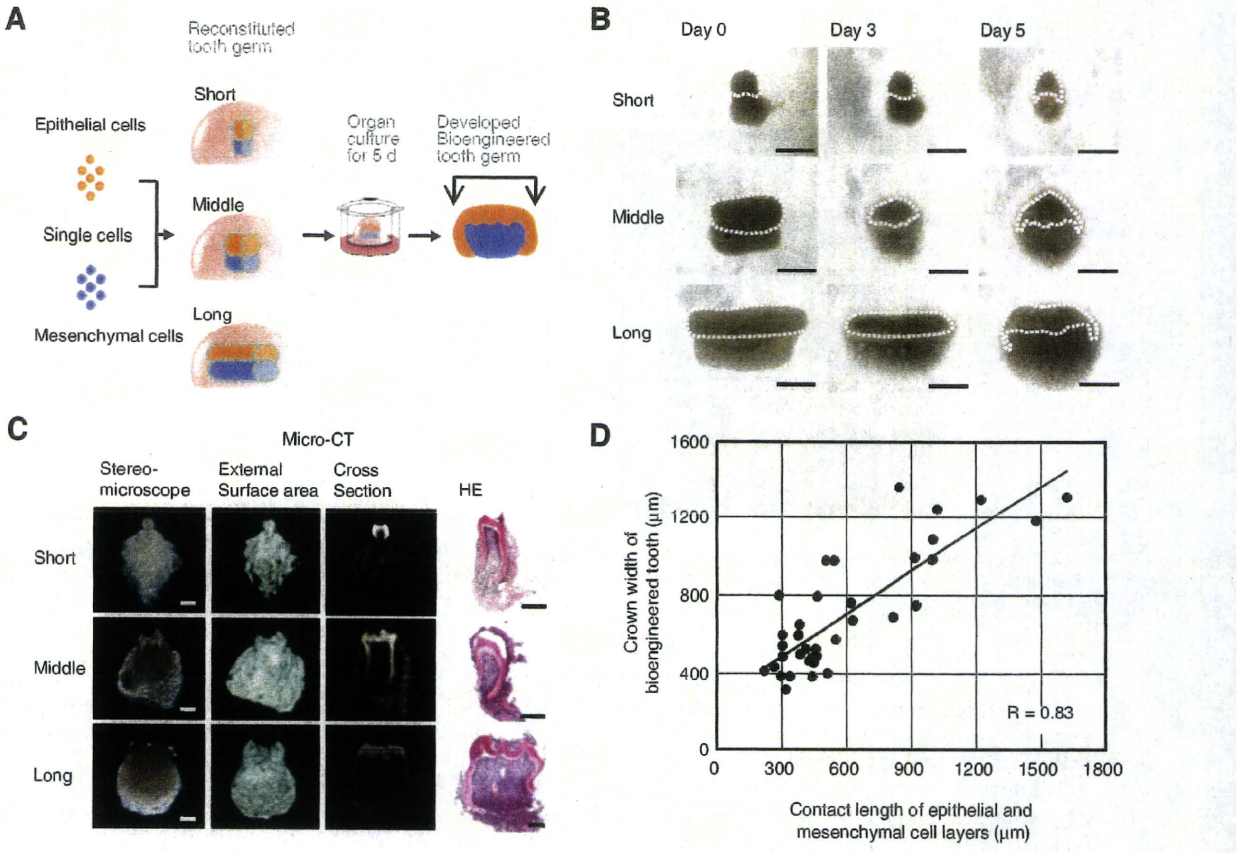

Fig. 1. The crown width of a bioengineered tooth correlates with the length of the contact area between the epithelial and mesenchymal cell layers. (A) Schematic representation of the bioengineering technology used for the generation of bioengineered tooth germ of various contact lengths between epithelial and mesenchymal cell layers. (B) Phase contrast images of the three contact area groups (upper, short; middle, middle; lower, long) of the bioengineered tooth germs on days 0, 3, and 5 of organ cultures. Scale bars, 200 μm. (C) Representative images of the three contact area bioengineered tooth groups (upper, short; middle, middle; lower, long) developed in a subrenal capsule environment for 21 days. Stereomicroscope (first columns from the left), external images (second columns) and cross sections (third columns) of Micro CT and hematoxylin and eosin staining (fourth columns) are shown. Scale bars, 200 μm. (D) Scatter diagram showing correlations between the contact lengths between epithelial and mesenchymal cells and the crown widths of the resulting bioengineered tooth ($R = 0.83$).

transplantation were then plotted and statistical analysis indicated a reliable correlation between the contact lengths of the bioengineered tooth germs and the crown widths of the resulting teeth ($R = 0.83$; Fig. 1D). These results indicate that the crown width is controlled by the contact area between the epithelial and mesenchymal cell layers.

3.2. The cusp number of the bioengineered teeth correlates with their crown width

We next examined whether the crown width affects the determination of the cusp number in the bioengineered teeth. At 21 days post-transplantation into the subrenal capsule, the cusp numbers of the bioengineered teeth were analyzed by Micro-CT (Fig. 2A). Statistical analysis indicated a reliable correlation between the contact length of the bioengineered tooth germs and the resulting cusp numbers of the bioengineered teeth ($R = 0.87$; Fig. 2B). These observations suggest that the eventual cusp number is indeed dependent on the crown width.

3.3. The Shh expression area correlates with the crown width in developing tooth germ

Sonic hedgehog (*Shh*) and *fibroblast growth factor 4* (*Fgf4*) play important roles in the early development of tooth germ [1,2]. We next investigated the expression patterns of these factors during the early developmental stages of both natural molar and bioengineered tooth germ. During natural tooth germ development, *Shh* and *Fgf4* mRNA-positive cells can be observed in the enamel knot, which is the epithelial signaling center, at ED13.5 and ED14.5 (Fig. 3A). Interestingly, the *Shh* expression area was found to extend from the enamel knot to the inner enamel epithelium, in accordance with the progression of crown development, but was restricted in the inner enamel epithelium at the prospective occlusal region, but not at the lateral region, at ED15.5 and ED16.5 (Fig. 3A). In contrast, *Fgf4* mRNA-positive cells were found to be restricted locally throughout the early period of crown development and these transcripts were detectable in the enamel knot at ED13.5–ED15.5 and in the secondary enamel knot at ED16.5 (Fig. 3A). In the case of the bioengineered molar germ, the expression patterns of *Shh* and *Fgf4* mRNAs were identical to those of the natural tooth germ (Fig. 3A). *Shh* expression was restricted to the enamel knot after 2 days and to the inner enamel epithelium at the prospective occlusal region after 3–7 days of organ culture (Fig. 3A). *Fgf4* expression was detected in the enamel knot after 3–5 days and in the secondary enamel knot after 7 days organ culture (Fig. 3A). The expression of *Fibroblast growth factor 3* (*Fgf3*), which is also thought to be an important mesenchymal signaling molecule, was detectable in the dental papillae adjacent to the *Shh*-expressing inner enamel epithelium throughout the early period of development in both natural and bioengineered tooth germ (Fig. 3B). Hence, although the development of bioengineered tooth

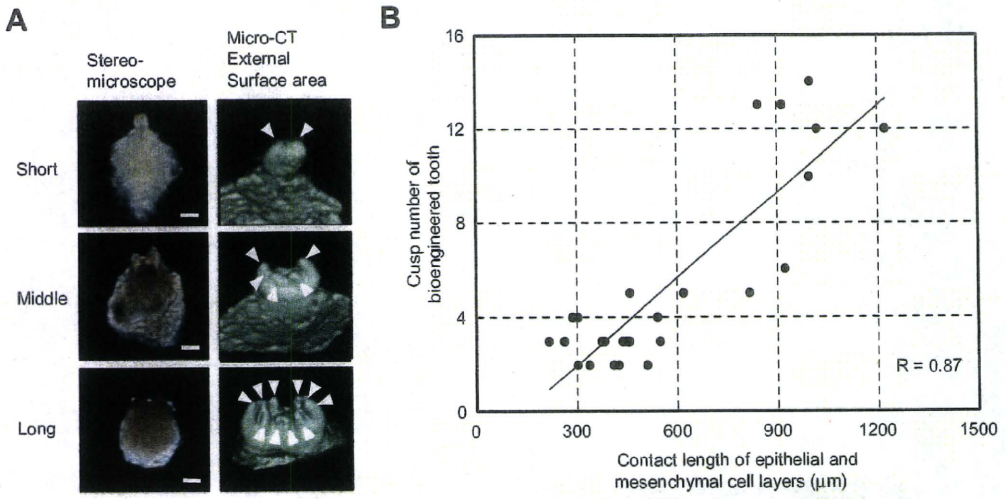

Fig. 2. The cusp number of the bioengineered tooth correlates with its crown width. (A) Stereomicroscope (left) and Micro CT (right) images of bioengineered teeth from the three contact area groups. Cusps are indicated by arrowheads. Scale bars, 200 μm. (B) Scatter diagram analysis of the correlation between the crown width and cusp number in bioengineered teeth ($R = 0.87$).

germ is delayed compared with natural germ, the molecular mechanisms regulating early tooth germ development are similar for both bioengineered and natural tooth germ.

We further examined the correlation between the width of *Shh*-expressing area in the inner enamel epithelium at the prospective occlusal region and the crown width of the bioengineered tooth germ. We generated bioengineered molar tooth germs from the three contact area groups over three days in organ culture. The *Shh*-expression area was found to be extended from the enamel knot to the inner enamel epithelium at the prospective occlusal region, but not at the lateral region, over the culture period, and the width of this area was observed to be equivalent to the width of prospective crown of bioengineered tooth germ (Fig. 3C). These results suggest that the *Shh*-expression pattern in the inner enamel epithelium is closely associated with the mechanisms that regulate crown width.

3.4. The spatiotemporal epithelial cell growth that correlates with the Shh expression pattern is involved in the regulation of crown size

We finally investigated whether the spatiotemporal *Shh* expression pattern shown in Fig. 3 is involved in the patterning of epithelial cell proliferation during tooth germ development. We therefore analyzed *Shh* expression using a transgenic mouse expressing green fluorescent protein (GFP) at the *Shh* locus (*ShhGFP* mice). We measured cell proliferation by immunohistochemical analysis of Ki67 in natural and bioengineered tooth germs. In a natural ED14.5 molar tooth germ, *Shh* expression in an *in vitro* organ culture shows the same expression pattern as that detected by *in situ* hybridization *in vivo* (Figs. 3A and 4A). Cell proliferation in natural tooth germ detected by Ki67 was evident at the cervical loop after one day and the lateral region of the epithelium after 2–4 days, in which *Shh* expression was not found (Fig. 4A). The bioengineered molar tooth germ showed expression of *Shh* at the first enamel knot on day 3 and in the inner enamel epithelium in the prospective occlusal region at day 6 in an organ culture. Cell proliferation of the bioengineered germ was also observed in the *Shh* expression-negative regions at the cervical loop and inner enamel epithelium in the lateral region after 6 days of organ culture (Fig. 4B). These results suggest that the crown width is determined by the spatiotemporal area patterning of the *Shh* expression-positive and cell proliferation-negative regions of the inner enamel epithelium during the early bell stage.

4. Discussion

We demonstrate herein that the crown width of a bioengineered tooth is regulated by the contact area between the epithelial and mesenchymal cell layers and associates with cell proliferation and *Shh* expression in the inner enamel epithelium. We also demonstrate that the cusp number is significantly correlated with the crown width of the bioengineered tooth. These findings also suggest that the spatiotemporal patterning of the cell proliferation and *Shh* expression areas in epithelium regulates the crown width and cusp formation of the tooth.

At the initiation phase of tooth germ development, the tooth-forming field and the basic pattern of dentition (molar and incisor) are regulated by the coordination of gene expression patterning [3]. Rostral–caudal patterning determines the tooth-forming field through the expression patterns of *Lhx6/7* and *Gsc* [3]. On the other hand, proximal-distal patterning determines the molar and incisor fields through the formation of gene expression patterning between *Bmp4* and *Fgf8* in the epithelium, and these gene products then induce *Msx1/2*, *Barx1* and *Dlx2* in the mesenchyme [3]. It is thought that the number of teeth, the sizes of which are also determined by the size of the tooth germ, is proportional to the size of the tooth-forming field [3]. A previous study has indicated that the final crown size is memorized in the dental mesenchyme and regulated by the reaction-diffusion model [10]. In our current study, we provide evidence that the crown width is determined by the contact area between the epithelial and mesenchymal cell layers. We also demonstrate that the *Shh*-expressing region in the dental epithelium of not only natural but also the bioengineered tooth germ gradually enlarges to the final size of the crown width, and that cell proliferation does not occur in the *Shh*-expression region. These findings indicate that cell proliferation is essential for the determination of the crown width in the inner enamel epithelium at the prospective occlusal region, in which the cells express *Shh*, and also for tooth root formation in the cervical loop region. It has been reported previously that *Shh* regulates epithelial proliferation, cell survival, and tooth size [15]. Our present results suggest the possibility that the spatiotemporal regulation of

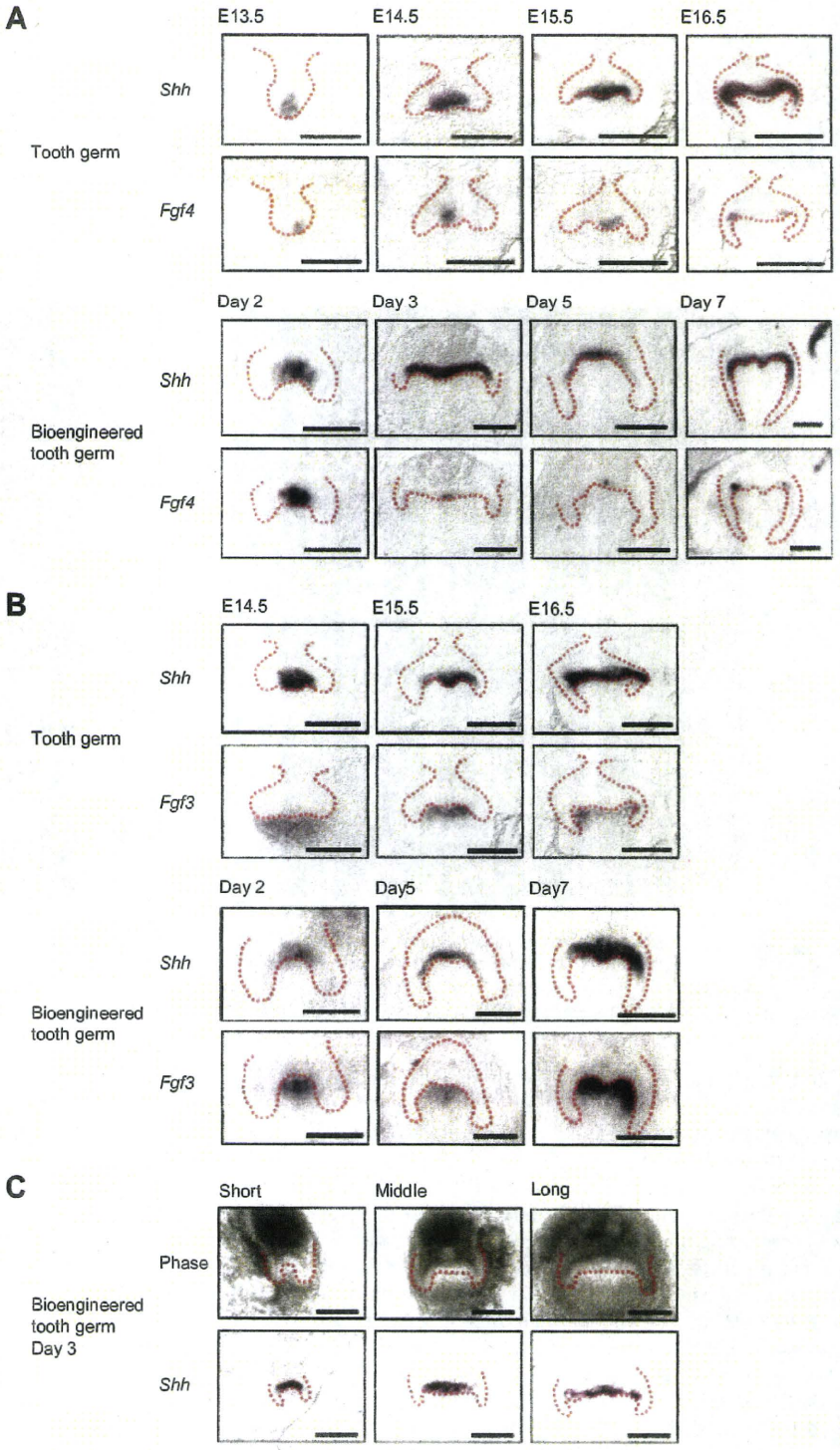

Fig. 3. The width of the *Shh* expression area correlates with the crown width in the developing tooth germ. (A) *In situ* hybridization analyses of the *Shh* and *Fgf4* expression profiles in natural tooth germ at ED13.5–ED16.5 and in bioengineered tooth germ after 2, 3, 5, and 7 days of organ culture. (B) Expression patterns of *Shh* and *Fgf3* in natural tooth germ at ED14.5–ED16.5 and bioengineered tooth germ after 2, 5, and 7 days of organ culture. (C) Phase contrast images and expression analysis of *Shh* mRNA in the three contact area groups of bioengineered tooth germ after three days of cultivation. Dotted lines indicate the boundaries between the epithelium and mesenchyme. The area inside the line is the epithelium. Scale bars, 200 μm.

epithelial cell proliferation and *Shh* expression are closely involved in the determination of tooth macro-morphology and represent the molecular basis of tooth size determination.

A reaction-diffusion model has been predicted and analyzed in the patterning of micro-structures such as digits in limbs, feathers in skin, and cusps in tooth [11,16,17]. Previous studies have suggested that the number of digits in the mouse limb is regulated by not only the width of the mesoderm but also the length of the *Fgf4*-expressing apical ectodermal ridge, which is the signaling center in limb development [18]. In tooth development, it is thought that the cusp patterning is regulated by the secondary enamel knots, which is one of the signaling centers for cusp